

Neutral PtRh₂ and PtRh₄ Tetraalkynyl Complexes. X-ray Crystal Structures of {Pt(C≡CBu^t)₄[Rh₂(μ-X)(COD)₂]₂} (X = Cl, OH)

Irene Ara,[†] Jesús R. Berenguer,[‡] Juan Forniés,^{*,†} and Elena Lalinde^{*,‡}

Departamento de Química Inorgánica, Instituto de Ciencia de Materiales de Aragón, Universidad de Zaragoza-Consejo Superior de Investigaciones Científicas, 50009 Zaragoza, Spain, and Departamento de Química, Universidad de La Rioja, 26001 Logroño, Spain

Received March 27, 1997[⊗]

The reaction of 2 equiv of [Rh(COD)(acetone)₂]⁺ with the dianionic homoleptic species [Pt(C≡CR)₄]²⁻ (R = Bu^t (**1a**), SiMe₃ (**1b**)) in acetone (molar ratio 2:1) gives the expected neutral trinuclear adducts {Pt(μ-C≡CR)₄[Rh(COD)]₂} (R = Bu^t (**2a**), SiMe₃ (**2b**)) in moderately good yield. Further reaction of **2a** with the binuclear [Rh(μ-X)(COD)]₂ (X = Cl, OH) derivatives (molar ratio 1:1) produces the formation of unusual pentanuclear {Pt(μ-C≡CBu^t)₄[Rh₂(μ-X)(COD)₂]₂} complexes (X = Cl (**3a**), OH (**4a**)), which are formed by a dianionic "Pt-(C≡CBu^t)₄" fragment and two dinuclear cationic "Rh₂(COD)₂(μ-X)" units connected through bridging alkynyl ligands. The molecular structures of complexes **3a** and **4a** have been established by X-ray crystallography.

Introduction

The chemistry of metal acetylide complexes has been the subject of intense study in recent years.¹ In this area a large number of studies involving the preparation and chemistry of homo- and heterobinuclear complexes stabilized by a double-alkynyl bridging system, L_nM(μ-C₂R)₂ML'_n, have been reported during the last decade and it now seems clear that the bonding of alkynyl ligands is a function of the nature of the R substituents and the organometallic termini.² In contrast to this, derivatives with a higher nuclearity and with the metal centers doubly bridged by alkynyl ligands have been explored to a much lesser extent.³

We have recently described the synthesis of tetraalkynylplatinate(II) species (NBu₄)₂[Pt(C≡CR)₄]_nH₂O (**1**: R = Bu^t (**1a**), SiMe₃ (**1b**), n = 2; R = Ph (**1c**), n = 0) and studied their ability to act as precursors in the preparation of homo- and heterotrinuclear complexes

containing four bridging alkynides.⁴ These homoleptic species **1** have therefore been used as starting materials in the construction of triplatinum anionic complexes [Pt₃(C₆F₅)₄(μ-C≡CR)₄]²⁻ (Chart 1, A) containing simultaneously both chelating and σ, π double-alkynyl bridging systems^{4a} and have been shown to react with mercury dihalides^{4b} (Chart 1, B), yielding simple bis-(η²-alkynyl)mercury(II) 1:2 adducts, {Pt(μ-C≡CR)₄-(HgX₂)₂]²⁻. We have found, however, that similar reactions with MX (M = Ag, Cu, X = Cl, Br) strongly depend on the nature of the R substituents. Thus, while treatment of the phenylacetylide complex **1** (R = Ph) with MX in a 1:2 molar ratio results in the formation of the expected trinuclear anionic species in which the "Pt-(C≡CPh)₄" fragment chelates two neutral MX units (Scheme 1, B), as was demonstrated by X-ray diffraction analysis,^{4c} similar reactions with [Pt(C≡CBu^t)₄]²⁻ yield hexametallallic species.

Continuing our work in this field, in this paper we report the neutralization reactions of **1** with 2 equiv of the cationic rhodium(I) solvento species [Rh(COD)(acetone)₂]⁺, which allow the synthesis and characterization of the first trinuclear {Pt(μ-C≡CR)₄[Rh(COD)]₂} (R = Bu^t (**2a**), SiMe₃ (**2b**)) neutral derivatives with two double-alkynyl bridging systems connecting the metal centers. In addition, complex **2a** is a precursor of higher nuclearity PtRh₄ compounds in which the dianionic [Pt-(C≡CBu^t)₄] entity remains intact.

Results and Discussion

Reaction of (NBu₄)₂[Pt(C≡CR)₄]₂H₂O (R = Bu^t, SiMe₃) with 2 equiv of the solvento complex [Rh(COD)(acetone)₂]⁺ (prepared *in situ*) affords the expected trinuclear {Pt(C≡CR)₄[Rh(COD)]₂} complexes (R = Bu^t (**2a**), SiMe₃ (**2b**)), which can be isolated as air-stable orange microcrystalline solids in moderately good yield (67%, **2a**; 77%, **2b**) (Scheme 1, i) and which have been characterized by means of the usual analytical and

[†] Universidad de Zaragoza-Consejo Superior de Investigaciones Científicas.

[‡] Universidad de La Rioja.

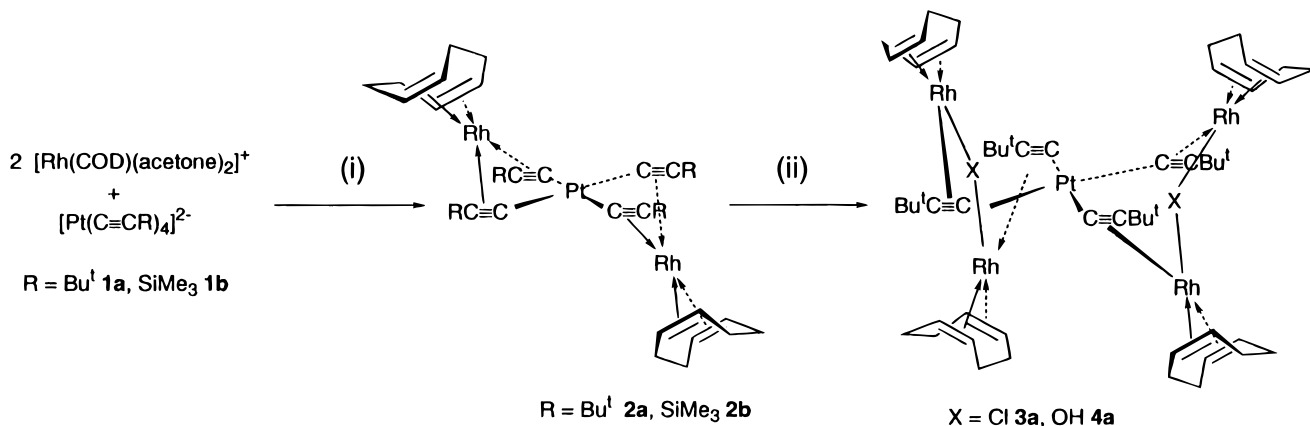
[⊗] Abstract published in *Advance ACS Abstracts*, August 1, 1997.

(1) (a) Nast, R. *Coord. Chem. Rev.* **1982**, *47*, 89. (b) Bruce, M. I. *Chem. Rev.* **1983**, *83*, 203. (c) Akita, M.; Moro-Oka, Y. *Bull. Chem. Soc. Jpn.* **1995**, *68*, 420. (d) Manna, J.; Jonh, K. D.; Hopkins, M. D. *Adv. Organomet. Chem.* **1996**, *79*.

(2) (a) Beck, W.; Niemer, B.; Wieser, M. *Angew. Chem., Int. Ed. Engl.* **1993**, *32*, 923. (b) Lotz, S.; Van Rooyen, P. H.; Meyer, R. *Adv. Organomet. Chem.* **1995**, *37*, 219. (c) Lang, H.; Köhler, K.; Blau, S. *Coord. Chem. Rev.* **1995**, *143*, 113. (d) Pavan Kumar, P. N. V.; Jemmins, D. *J. Am. Chem. Soc.* **1988**, *110*, 125. (e) Rosenthal, U.; Pulst, S.; Arndt, P.; Ohff, A.; Tillack, A.; Baumann, W.; Kempe, R.; Burlakov, V. V. *Organometallics* **1995**, *14*, 2961. (f) Varga, V.; Mach, K.; Hiller, J.; Thewalt, U.; Sedmera, P.; Polásek, M. *Organometallics* **1995**, *14*, 1410. (g) Erker, G.; Albrecht, M.; Nolte, M.; Werner, S. *Organometallics* **1993**, *12*, 4979. (h) Lee, L.; Berg, D. J.; Bushnell, G. W. *Organometallics* **1995**, *14*, 5021. (i) Chang, C. C.; Srinivas, B.; Wu, M. L.; Chiang, W. H.; Chiang, M. Y.; Hsiung, C. S. *Organometallics* **1995**, *14*, 5150. (j) Janssen, M. D.; Köhler, K.; Herres, M.; Dedin, A.; Smeets, W. J. J.; Spek, A. L.; Grove, D. M.; Lang, H.; van Koten, G. *J. Am. Chem. Soc.* **1996**, *118*, 4817. (k) Forniés, J.; Lalinde, E. *J. Chem. Soc., Dalton Trans.* **1996**, 2587 (Perspective).

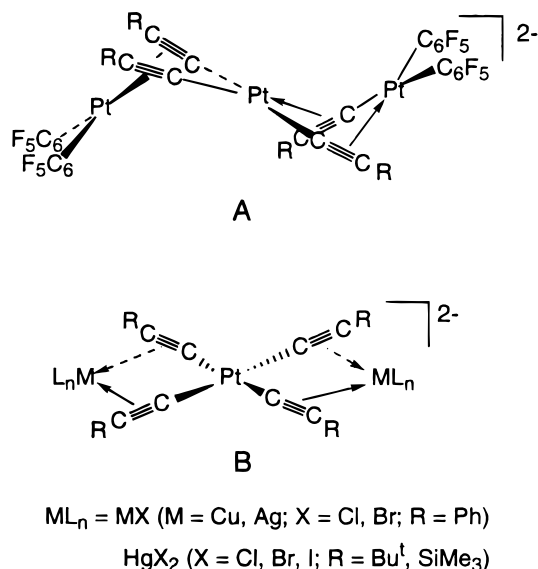
(3) (a) Boncella, J. M.; Tilley, T. D.; Andersen, R. A. *J. Chem. Soc., Chem. Commun.* **1984**, 710. (b) Yamazaki, S.; Deeming, A. J. *J. Chem. Soc., Dalton Trans.* **1993**, 3051. (c) Edwards, A. J.; Fallaize, A.; Raithby, P. R.; Rennie, M. A.; Steiner, A.; Verhovevoort, K. L.; Wright, D. S. *J. Chem. Soc., Dalton Trans.* **1996**, 133. (d) Kawaguchi, H.; Tatsumi, K. *Organometallics* **1995**, *14*, 4294.

(4) (a) Forniés, J.; Lalinde, E.; Martín, A.; Moreno, M. T. *J. Chem. Soc., Dalton Trans.* **1994**, 135. (b) Berenguer, J. R.; Forniés, J.; Lalinde, E.; Martín, A.; Moreno, M. T. *J. Chem. Soc., Dalton Trans.* **1994**, 3343. (c) Forniés, J.; Lalinde, E.; Martín, A.; Moreno, M. T. *J. Organomet. Chem.* **1995**, *490*, 179.

Scheme 1^a

^a Legend: (i) acetone, 10 min; (ii) +2[Rh(μ -X)(COD)]₂ (**3a**, Et₂O; **4a**, THF).

Chart 1



spectroscopic techniques. Attempts to obtain the analogous derivative **2c** have been unsuccessful: the reaction of the substrate (NBu₄)₂[Pt(C≡CPh)₄] (**1c**) and [Rh(COD)(acetone)₂]⁺ under the same conditions as those used for **2a,b** only affords a mixture of unidentified decomposition products as a black solid from which we were not able to separate any pure compound. Unambiguous structural characterization of complexes **2** has not been achieved, as all our attempts to obtain suitable crystals for X-ray analysis have been unsuccessful. Their spectroscopic data are, however, consistent with a **B** type formulation (Chart 1), in which the tetraalkynylplatinate fragment acts as a chelating bridging ligand toward two Rh(COD) units. Although there are many reported examples in which unsaturated ML_n fragments are well-embedded between the two arms of metalladiyne species displaying planar MC₄M' cores,^{2c,j} the same structure seems unlikely in these derivatives (**2**) because of steric reasons. Due to the expected perpendicular orientation of the acetylenic fragments to the rhodium(I) coordination plane we propose the structure shown in Scheme 1 and a bent conformation of the Pt(acetylide)₂Rh^I cores as the most probable arrangement. Nonplanar MC₄M' cores have been previously observed with platinum and palladium(II) organometallic fragments coordinated to metalladiyne chelating units.⁵ As expected for the proposed structure, their IR spectra exhibit two $\nu(\text{C}\equiv\text{C})$ absorptions (2039 (w),

2016 (w) cm⁻¹; **2a**; 1965 (vs), 1948 (vs) cm⁻¹; **2b**) shifted to lower wavenumbers with respect to those observed for the corresponding mononuclear precursor (2075, 2081 cm⁻¹, **1a**; 2015, 1981 (sh) cm⁻¹, **1b**) and the room- and low-temperature ¹H NMR spectra are very simple, showing the equivalence of the two COD groups and the four alkynyl ligands (see Experimental Section). The expected asymmetry of the COD ligands is not, however, reflected in solution. Even at low temperature both complexes show only one type of olefinic proton and carbon resonance in the ¹H and ¹³C{¹H} NMR spectra, respectively. In the case of complex **2b** the two sharp signals of the diene ligands (δ 82.01 d, ¹J_{Rh-C} = 11.3 Hz, olefinic; δ 30.92 s, aliphatic) observed at room temperature in the ¹³C NMR spectrum broaden upon cooling at -50 °C (δ 79.7 br, 31.06 br). This broadening suggests the occurrence of a dynamic process which is probably averaging the *endo* and *exo* olefinic carbons (and the aliphatic atoms as well) on each COD ligand that would be expected for a bent conformation on the Pt(acetylide)₂Rh cores. The ¹³C NMR spectra of complexes **2** reveal that upon η^2 coordination of the alkyne ligands to the rhodium atoms the signals due to the C _{α} and C _{β} atoms of the Pt-C≡C entity (98.9 and 108.4 ppm in **1a** and 140.4 and 104.4 ppm in **1b**) shift upfield for C _{α} and downfield for C _{β} . This result contrasts with previous observations showing that η^2 complexation of terminal alkynyl ligands to a second metal center results in a downfield shift of both the C _{α} and C _{β} resonances.^{2c,j,6} For **2b** the signals appear as pseudotriplets (1:4:1) showing coupling to only ¹⁹⁵Pt nuclei (δ C _{α} 123.93, ¹J_{Pt-C α} = 752.2; C _{β} 105.99, ²J_{Pt-C β} = 235 Hz). In the case of complex **2a**, the η^2 -bonded alkyne signals at 92.19 ppm (C _{α}) and 110.97 ppm (C _{β}) are seen as doublets resulting from ¹J_{¹³C-¹⁰³Rh} values of 4.6 and 4.5 Hz, respectively, flanked by ¹⁹⁵Pt satellites (¹J_{Pt-C α} = 911 Hz; ²J_{Pt-C β} = 269.6 Hz). Both the ¹J_{Pt-C α} and ²J_{Pt-C β} platinum coupling constants are notably smaller in these complexes **2a,b** than those observed in the precursors (975 and 279 Hz, respectively, in **1a** and 924

(5) (a) Forniés, J.; Gómez-Saso, M. A.; Lalinde, E.; Martínez, F.; Moreno, M. T. *Organometallics* **1992**, *11*, 2873. (b) Berenguer, J. R.; Forniés, J.; Lalinde, E.; Martínez, F. *J. Organomet. Chem.* **1994**, *470*, C15. (c) Berenguer, J. R.; Forniés, J.; Lalinde, E.; Martínez, F. *J. Chem. Soc., Chem. Commun.* **1995**, 1227. (d) Berenguer, J. R.; Forniés, J.; Lalinde, E.; Martínez, F. *Organometallics* **1996**, *15*, 4537.

(6) (a) Erker, G.; Frömberg, W.; Benn, R.; Mynott, R.; Angermund, K.; Krüger, C. *Organometallics* **1989**, *8*, 911. (b) Lang, H.; Blau, S.; Nuber, B.; Zsolnai, L. *Organometallics* **1995**, *14*, 3216 and references given therein. (c) Lang, H.; Blau, S.; Pritzkow, H.; Zsolnai, L. *Organometallics* **1995**, *14*, 1850.

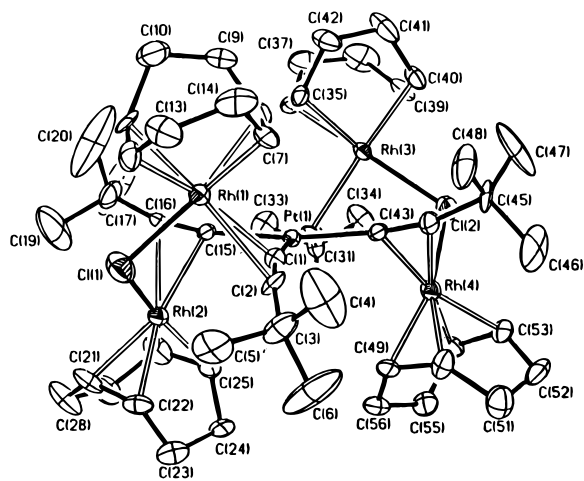


Figure 1. Structure of $\{\text{Pt}(\text{C}\equiv\text{CBu}^t)_4[\text{Rh}_2(\mu\text{-Cl})(\text{COD})_2]_2\}$ (**3a**) showing the atom-labeling scheme. Ellipsoids are drawn at the 35% probability level.

and 250.4 Hz in **1b**). This fact has been previously observed^{5d} in related Pt–Pd and Pd–Pt–Pd complexes containing alkynyl bridging ligands $[\text{Pt}(\mu\text{-}\kappa^1\text{:}\eta^2\text{-C}\equiv\text{CR})\text{-Pd}]$ and clearly reflects the expected lower degree of s orbital participation in the platinum–carbon alkynyl bridging bond due to a partial rehybridization of the carbon atoms toward sp^2 . The values of the variation in $\Delta J_{\text{Pt-C}}$ are considerably smaller in complex **2a**, suggesting a weaker (η^2 -alkyne)rhodium interaction. In support of this observation we have found that complex **2b** is more stable in solution than **2a**. In addition, while complex **2a** easily reacts with $[\text{RhX}(\text{COD})_2]$ ($X = \text{Cl}, \text{OH}$), yielding the pentanuclear derivatives (**3a** and **4a**), the derivative **2b** is inert under similar conditions. It should also be mentioned that the synthesis of complex **2a** is very sensitive to traces of water in the acetone solvent. If the solvent used for its preparation is not carefully dried, variable mixtures of **2a**, **3a**, and **4a** are found in the reaction mixture.

As previously mentioned, the treatment of the *tert*-butylalkynyl derivative **2a** with 1 molar equiv of the binuclear chloride or hydroxo derivatives $[\text{RhX}(\text{COD})_2]$ ($X = \text{Cl}, \text{OH}$) affords the pentanuclear compounds $\{\text{Pt}(\mu\text{-C}\equiv\text{CBu}^t)_4[\text{Rh}_2(\mu\text{-X})(\text{COD})_2]_2\}$ ($X = \text{Cl}$ (**3a**), OH (**4a**)) (Scheme 1) containing the dianionic tetraalkynylplatinate fragment acting as a bridging tetradentate ligand toward two cationic dirhodium organometallic “ $\text{Rh}_2(\mu\text{-X})(\text{COD})_2$ ” units. Both compounds, **3a** and **4a**, are moderately air-stable orange crystalline solids, but they decompose slowly in chlorinated solvents. A definitive structural assignment which confirms the pentanuclear nature of both compounds and also indirectly supports the structure of the **2a** precursor has been obtained by single-crystal X-ray crystallography (Figures 1 and 2). Relevant bond distances and angles are given in Tables 1 and 2. These are the first structurally characterized compounds containing only alkynyl bridging ligands between Rh and Pt. In both derivatives the starting dianionic “ $\text{Pt}(\text{C}\equiv\text{CBu}^t)_4$ ” fragment acts as a tetradentate bridging ligand between two cationic dirhodium units through η^2 coordination of the alkynyl groups to each rhodium atom. In complex **4a** the two cationic “ $(\text{COD})\text{-Rh}(1)(\mu\text{-OH})\text{Rh}(2)(\text{COD})$ ” units are related by a crystallographic C_2 axis. In both molecules (**3a** and **4a**) the platinum and rhodium atoms exhibit conventional square-planar environments (see Figure 3) and each organometallic metal core shows the expected structural

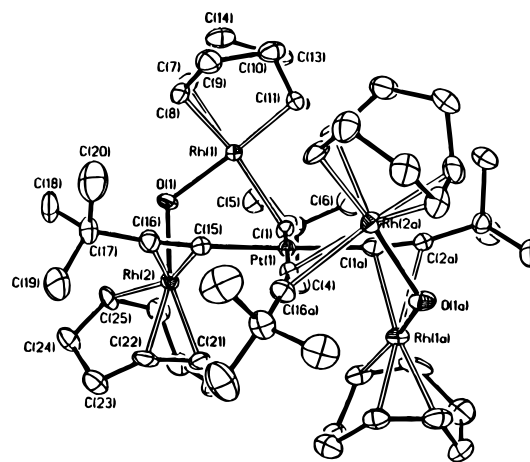


Figure 2. Molecular structure and atom-numbering scheme for $\{\text{Pt}(\text{C}\equiv\text{CBu}^t)_4[\text{Rh}_2(\mu\text{-OH})(\text{COD})_2]_2\}$ (**4a**). Ellipsoids are drawn at the 35% probability level.

Table 1. Selected Bond Distances (Å) and Angles (deg) for Complex **3a**

Pt(1)–C(1)	2.026(14)	Pt(1)–C(15)	2.010(12)
Pt(1)–C(29)	2.012(13)	Pt(1)–C(43)	2.004(12)
Rh(1)–C(1)	2.243(13)	Rh(1)–C(2)	2.391(12)
Rh(1)–C(7)	2.142(12)	Rh(1)–C(8)	2.105(12)
Rh(1)–C(11)	2.133(11)	Rh(1)–C(12)	2.111(13)
Rh(1)–Cl(1)	2.363(4)	Rh(2)–Cl(1)	2.391(4)
Rh(2)–C(15)	2.250(11)	Rh(2)–C(16)	2.418(11)
Rh(2)–C(21)	2.092(12)	Rh(2)–C(22)	2.132(13)
Rh(2)–C(25)	2.102(13)	Rh(2)–C(26)	2.119(12)
Rh(3)–C(29)	2.271(11)	Rh(3)–C(30)	2.456(11)
Rh(3)–C(35)	2.107(12)	Rh(3)–C(36)	2.118(12)
Rh(3)–C(39)	2.097(12)	Rh(3)–C(40)	2.116(12)
Rh(3)–Cl(2)	2.400(4)	Rh(4)–Cl(2)	2.403(4)
Rh(4)–C(43)	2.283(11)	Rh(4)–C(44)	2.403(12)
Rh(4)–C(49)	2.107(12)	Rh(4)–C(50)	2.123(13)
Rh(4)–C(53)	2.115(12)	Rh(4)–C(54)	2.148(11)
C(1)–C(2)	1.20(2)	C(15)–C(16)	1.22(2)
C(29)–C(30)	1.21(2)	C(43)–C(44)	1.22(2)
C(1)–Pt(1)–C(15)	96.3(5)	C(1)–Pt(1)–C(43)	83.5(5)
C(15)–Pt(1)–C(29)	86.4(4)	C(29)–Pt(1)–C(43)	95.0(4)
Rh(1)–Cl(1)–Rh(2)	109.8(2)	Rh(3)–Cl(2)–Rh(4)	104.46(13)
C(2)–C(1)–Pt(1)	165.7(11)	C(1)–C(2)–C(3)	166.5(14)
C(16)–C(15)–Pt(1)	170.0(10)	C(15)–C(16)–C(17)	166.4(13)
C(30)–C(29)–Pt(1)	171.6(10)	C(29)–C(30)–C(31)	167.1(12)
C(44)–C(43)–Pt(1)	171.5(11)	C(43)–C(44)–C(45)	163.8(13)

Table 2. Selected Bond Distances (Å) and Angles (deg) for Complex **4a**^a

Pt(1)–C(1)	2.018(9)	Pt(1)–C(15)	2.005(9)
Rh(1)–C(1)	2.266(9)	Rh(1)–C(2)	2.474(9)
Rh(1)–C(7)	2.116(10)	Rh(1)–C(8)	2.101(9)
Rh(1)–C(11)	2.116(9)	Rh(1)–C(12)	2.104(9)
Rh(1)–O(1)	2.112(6)	Rh(2)–O(1)	2.094(6)
Rh(2)–C(15)	2.253(8)	Rh(2)–C(16)	2.413(9)
Rh(2)–C(21)	2.104(9)	Rh(2)–C(22)	2.117(9)
Rh(2)–C(25)	2.081(9)	Rh(2)–C(26)	2.116(9)
C(1)–C(2)	1.200(11)	C(15)–C(16)	1.205(12)
C(1)–Pt(1)–C(15)	93.1(3)	C(1)–Pt(1)–C(1a)	87.1(5)
C(15)–Pt(1)–C(15a)	86.7(5)	Rh(2)–O(1)–Rh(1)	113.2(3)
C(2)–C(1)–Pt(1)	173.3(8)	C(1)–C(2)–C(3)	168.3(9)
C(16)–C(15)–Pt(1)	170.6(8)	C(15)–C(16)–C(17)	167.5(10)

^a Symmetry transformation used to generate equivalent atoms: $-x + 1, y, -z + 1/2$.

features. Bond lengths and angles around the platinum cores are thus all within the range found in other heteropolynuclear platinum acetylide compounds.^{4,5}

Each rhodium atom in the “ $\text{Rh}_2(\mu\text{-X})(\text{COD})_2$ ” units is η^2 -bonded to the two olefinic bonds of one cyclooctadiene ligand and to the carbon–carbon triple bond of one of the alkynyl groups and completes its coordination with a bridging X group ($X = \text{Cl}$ in **3a**, OH in **4a**). The Rh–O bond distances in **4a** ($\text{Rh}(1)\text{-O}(1) = 2.112(6)$ Å and $\text{Rh}(2)\text{-O}(1) = 2.094(6)$ Å) are comparable to those found

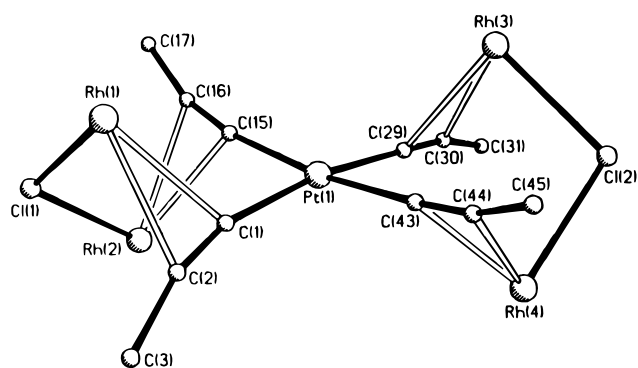


Figure 3. Schematic view of the central core of **3a**. Complex **4a** displays a very similar structure.

in $[\text{Rh}(\mu\text{-OH})(\text{COD})]_2$ ^{7b} and in other binuclear rhodium hydroxo complexes $[\text{Rh}(\text{OH})\text{L}_2]_2$ ($\text{L} = \text{PPh}_3$,^{7c} P^iPr_3 ^{7d}). Similarly, the Rh–Cl bonds in **3a** range from 2.363(4) to 2.403(4) Å, which are comparable to the value of 2.38 Å observed in $[\text{RhCl}(\text{COD})]_2$ ^{8c} and to those observed in other chloro-bridged binuclear rhodium complexes $[\text{RhClL}_2]_2$ ($\text{L} = \text{PPh}_3$,^{8d} P^iPr_3 ^{8e}). As a consequence of the η^2 interaction of the *tert*-butylalkynyl ligands with rhodium atoms, the Rh–Cl–Rh angles in **3a** (109.8(2) and 104.5(1)°) and the Rh(1)–O(1)–Rh(2) angle in **4a** (113.2(3)°) are notably larger than the corresponding ones observed in the dimeric complexes $[\text{Rh}(\mu\text{-X})(\text{COD})_2]$ ($\text{X} = \text{Cl}$, 94.4°;^{8c} $\text{X} = \text{OH}$, average 87.8°^{7b}).

The π -interactions between the acetylene fragments and the Rh atoms are rather unsymmetrical, the Rh–C $_{\alpha}$ distances (**3a**, range 2.24(1)–2.28(1) Å; **4a**, Rh(1)–C(1) = 2.266(9) Å, Rh(2)–C(15) = 2.254(8) Å) being significantly shorter than the corresponding Rh–C $_{\beta}$ distances (**3a**, range 2.39(1)–2.46(1) Å; **4a**, Rh(1)–C(2) = 2.474(9) Å, Rh(2)–C(16) = 2.413(9) Å). This type of asymmetry has been previously found in the mixed complex $[\text{ClPt}(\mu, \kappa^1\text{-}\eta^2\text{-C}_2\text{Me})(\mu\text{-dppm})_2\text{Rh}(\text{CO})](\text{PF}_6)$ ^{9a} and in the binuclear derivatives $[\text{Rh}_2(\text{CO})_2(\mu, \kappa^1\text{-}\eta^2\text{-C}_2\text{Bu}^t)(\text{dppm})](\text{ClO}_4)$,^{9b} $[\text{Rh}_2(\mu\text{-OOCFF}_3)(\mu, \kappa^1\text{-}\eta^2\text{-C}_2\text{Ph})(\text{CO})_2(\text{PCy}_3)_2]$,^{9c} and $[\text{RhIr}(\text{C}_2\text{Ph})(\text{CO})_2(\mu\text{-H})(\mu\text{-C}_2\text{Ph})(\text{dppm})_2](\text{CF}_3\text{SO}_3)$.^{9d} Moreover, the distance between the Rh atoms and the midpoints of the C≡C triple bonds is somewhat different. In complex **3a** these distances are Rh(1)–C(1,2) = 2.240(1) Å, Rh(2)–C(15,16) = 2.255(1) Å, Rh(3)–C(29,30) = 2.287(1) Å, and Rh(4)–C(43,44) = 2.263(1) Å. For the hydroxo derivative **4a**, the Rh(1)–C(1,2) and the Rh(2)–C(15,16) distances are 2.295(1) and 2.255(1) Å, respectively. The C≡C bond lengths in both complexes are identical within experimental error (see Tables 1 and 2).

In both molecules the rhodium atoms are located above (Rh(2) 1.583(1) Å and Rh(4) 1.377(1) Å in **3a** and Rh(1) 1.796(1) Å in **4a**) and below (Rh(1) 1.325(1) Å and

Rh(3) 1.692(1) Å in **3a** and Rh(2) 1.285(1) Å in **4a**) the platinum coordination planes and there is only a slight deviation of the acetylenic skeletons from linearity. Finally, the large separation between the platinum and the rhodium centers (range from 3.370(1) to 3.547(1) Å in **3a**; 3.315(1), 3.4246(1) Å and the Rh–Rh atoms in the trimetallacycles (Rh(1)⋯Rh(2) = 3.891(1) Å and Rh(3)⋯Rh(4) = 3.796(1) Å in **3a**; Rh(1)⋯Rh(2) = 3.512(1) Å in **4a**) clearly indicates that no metal–metal interactions are present.

In agreement with the structures shown in Figures 1 and 2, the IR spectra of **3a** and **4a** show only one absorption at 2022 (**3a**) and 2021 cm^{-1} (**4a**) attributable to $\nu(\text{C}\equiv\text{C})$ in the expected region for bridging alkynyl ligands. In addition, in the IR spectrum of **4a** a sharp absorption of medium intensity at 3602 cm^{-1} is observed, which is consistent with the presence of hydroxo groups. The ¹H NMR spectra clearly indicate that both complexes are involved in dynamic processes. Thus, the high-temperature (30 °C) ¹H NMR spectrum of **3a** exhibits, in addition to a single resonance (δ 1.51) due to Bu^t groups, three signals only: one broad signal in the olefinic region (δ 4.61, 16H) and two in the aliphatic proton range (δ 2.39, 16H; δ 1.74, 16H), due to the COD ligands. The olefinic and aliphatic resonances clearly broaden as the temperature is lowered,¹⁰ and at –50 °C the spectrum shows the four different olefinic and four aliphatic resonances expected in the low-exchange region. The ¹H NMR spectrum of **4a** displays, at room temperature, two olefinic and two aliphatic resonances which only broaden at low temperature (–50 °C). These signals can be assigned to the protons of each carbon–carbon double bond (*trans* to hydroxo and *trans* to the acetylenic fragment), suggesting the existence of a fluxional process which averages the *endo* and *exo* protons of the diolefin. The fluxional process could involve a rapid ring inversion of the six-membered Pt-(acetylenic)₂Rh₂O metallacycles, producing the observed time-averaged plane of symmetry on the rhodium centers. For complex **3a** the observation of only one olefinic resonance at 30 °C suggests that an additional dynamic process occurs, probably *via* tricoordinated rhodium intermediates, which involves the relative positions of both carbon–carbon double bonds.

In the ¹³C NMR spectra the most remarkable features are the alkynyl carbon resonances, which are seen as singlets with satellites due to the ¹⁹⁵Pt isotope. Both C $_{\alpha}$ (80.98 ppm, **3a**; 78.83 ppm, **4a**) and C $_{\beta}$ (102.14 ppm, **3a**; 106.69 ppm, **4a**) signals have undergone a notable upfield shift with respect to the starting precursor **2a**, while the magnitude of the platinum coupling constants is only slightly increased (see Experimental Section).

Conclusion

In conclusion, we have demonstrated that both trinuclear (PtRh₂) and pentanuclear (PtRh₄) tetraalkynyl complexes can be prepared from easily available tetraalkynyl dianionic $[\text{Pt}(\text{C}\equiv\text{CR})_4]^{2-}$ precursors. It is important to remark that in the formation of complexes **2**, **3a**, and **4a**, the platinum centers retain the σ -coordination to the alkynyl groups. No alkylation processes have been observed in any of the cases, in spite of the fact that electrophilic cationic rhodium complexes

(10) Within the +15 to –50 °C range the olefinic resonances practically do not merge from the base line.

(7) Preparation: (a) Usón, R.; Oro, L. A.; Cabeza, J. A. *Inorg. Synth.* **1985**, *23*, 126. X-ray structure: (b) Selent, D.; Ramm, M. *J. Organomet. Chem.* **1995**, *485*, 135. (c) Brune, H.-A.; Hemmer, R.; Unsin, J.; Holl, K.; Thewalt, Z. *Z. Naturforsch.* **1988**, *43B*, 487. (d) Gevert, O.; Wolf, J.; Werner, H. *Organometallics* **1996**, *15*, 2806.

(8) Preparation: (a) Chatt, J.; Venanzi, L. M. *J. Chem. Soc.* **1957**, 4735. (b) Giordano, G.; Crabtree, R. H. *Inorg. Synth.* **1990**, *28*, 88. X-ray structure: (c) Ibers, J. A.; Snyder, R. G. *Acta Crystallogr.* **1962**, *15*, 923. (d) Curtis, M. D.; Butler, W. M.; Greene, J. *Inorg. Chem.* **1978**, *17*, 2928. (e) Binger, P.; Haas, J.; Glaser, G.; Goddard, R.; Krüger, C. *Chem. Ber.* **1994**, *127*, 1927.

(9) (a) Hutton, A. T.; Shebanzadeh, B.; Shaw, B. L. *J. Chem. Soc., Chem. Commun.* **1984**, 549. (b) Cowie, M.; Loeb, S. *Organometallics* **1985**, *4*, 852. (c) Esteruelas, M. A.; Lahuerta, O.; Modrego, J.; Nürnberg, O.; Oro, L. A.; Rodríguez, L.; Sola, E.; Werner, H. *Organometallics* **1993**, *12*, 266. (d) Antwi-Nsiah, H. F.; Oke, O.; Cowie, M. *Organometallics* **1996**, *15*, 506.

have been used in the reactions. This fact is surprising and contrasts with the monoalkynylation processes observed in the formation of [Pt₃(C₆F₅)₄(μ-C≡CR)₄]²⁻ (Chart 1, A) starting from **1** and 2 equiv of the neutral substrate *cis*-[Pt(C₆F₅)₂(THF)₂].^{4a}

Similar alkynylation processes have also been observed with the mixed dianionic species [*cis*-Pt(C₆F₅)₂(C≡CR)₂]²⁻. Thus, binuclear derivatives containing σ, π double-alkynyl bridging systems such as [(C₆F₅)₂Pt(μ-κ¹:η²-C≡CR)(μ-η²:η¹-C≡CR)ML₂]ⁿ⁻ (ML₂ = Pt(C₆F₅)₂, Pd(C₆F₅)₂, n = 2;^{5a} Ir(COD), n = 1¹¹) are obtained with [*cis*-Pt(C₆F₅)₂(C≡CR)₂]²⁻ as starting material through monoalkynylation processes. As we have previously pointed out,^{5a} these alkynylation processes could be driven because of the difference in the formal charge of the metal centers involved.

The nature of the metal centers and/or the R substituent on the alkynyl ligand would, however, also seem to play a decisive role. Thus, whereas [*cis*-Pt(C₆F₅)₂(C≡CSiMe₃)₂]²⁻ reacts with the rhodium solvento complex [RhCp*(PEt₃)(acetone)₂]²⁺, yielding the neutral zwitterionic derivative [(C₆F₅)₂Pt(μ-κ¹:η²-C≡CSiMe₃)(μ-η²:κ¹-C≡CSiMe₃)Rh⁺Cp*(PEt₃)] through a monoalkynylation process,¹² the reaction between [*cis*-Pt(C₆F₅)₂(C≡CPh)₂]²⁻ and the analogous iridium solvento complex [IrCp*(PEt₃)(acetone)₂]²⁺ yields, through an unexpected double-alkynylation process, the binuclear derivative {[Cp*(PEt₃)Ir(C≡CPh)]Pt(C₆F₅)₂]^{5c} in which the resulting neutral unit "Cp*(PEt₃)Ir(κ¹-C≡CPh)₂" acts as a chelating ligand toward the "*cis*-Pt(C₆F₅)₂" platinum fragment. The final bonding preference (σ or π) of the metal centers to the alkynyl groups in these species containing double (μ-C≡CR)₂ bridging systems seems to be the result of a compromise of steric and electronic factors. Work in progress is mainly aimed at answering all these questions.

Experimental Section

All reactions have been carried out under a nitrogen atmosphere. Acetone was treated with KMnO₄ and distilled prior to use. (NBu₄)₂[Pt(C≡CR)₄]·nH₂O (n = 0, R = Ph;¹³ n = 2, R = Bu^t,¹³ SiMe₃^{4a}) and [Rh(μ-X)(COD)]₂ (X = Cl,^{8a,b} OH^{7a}) were prepared by published methods. NMR spectra were recorded on a Bruker ARX-300 spectrometer and IR spectra on a Perkin-Elmer 883 spectrometer using Nujol mulls between polyethylene sheets. Elemental analyses were carried out with a Perkin-Elmer 240 microanalyzer, and mass spectra were recorded on a VG Autospec double-focusing mass spectrometer operating in the FAB⁺ mode.

Preparation of {Pt(μ-C≡CR)₄[Rh(COD)]₂} (R = Bu^t (2a**), SiMe₃ (**2b**)).** A yellow solution of [Rh(μ-Cl)(COD)]₂ (0.320 g, 0.75 mmol for **2a**; 0.20 g, 0.406 mmol for **2b**) in acetone (20 cm³) was treated with AgClO₄ (0.313 g, 1.50 mmol for **2a**; 0.168 g, 0.811 mmol for **2b**), and the mixture was stirred at room temperature overnight and filtered through Celite. The resulting yellow solution, which contains [Rh(COD)(acetone)₂](ClO₄), was concentrated to ca. 10 cm³ and cooled to 0 °C; subsequently, (NBu₄)₂[Pt(C≡CR)₄]·2H₂O (0.78 g, 0.75 mmol for R = Bu^t or 0.445 g, 0.403 mmol for R = SiMe₃) was added to immediately give a deep orange solution. After the mixture was stirred for 10 min, evaporation of the solvent to a small

volume (ca. 3 cm³) and cooling in the freezer afforded complexes **2** as orange solids, which were filtered and washed with EtOH. Yields: **2a**, 0.47 g (67%); **2b**, 0.31 g (77%).

Data for **2a** are as follows. Anal. Calcd for C₄₀H₆₀PtRh₂: C, 51.02; H, 6.37. Found: C, 50.67; H, 6.22. MS (FAB⁺): *m/z* 941 (M⁺, 20%), 833 (M⁺ - COD, 36%). IR (cm⁻¹): ν(C≡C) 2039 (w), 2016 (w). ¹H NMR (CDCl₃, δ, 15 °C): 4.85 (s, br, 8H, COD, olefinic), 2.42 (br, 8H, COD, methylene), 1.86 (d, br, 8H, COD, methylene), 1.29 (s, 36H, Bu^t); a similar pattern was observed at -50 °C, 4.8 (s, br, 8H, COD, olefinic), 2.38 (br, 8H, COD, methylene), 1.83 (br, 8H, COD, methylene), 1.25 (s, 36 H, Bu^t). ¹³C NMR (CDCl₃, δ, -50 °C): 110.97 (d, C_β, C_α≡C_βBu^t, J_{Rh-C} = 4.5 Hz, ²J_{Pt-C} = 269.6 Hz), 92.19 (d, C_α, C_α≡C_βBu^t, J_{Rh-C} = 4.6 Hz, ¹J_{Pt-C} = 911 Hz), 76.98 (d, COD, olefinic, J_{Rh-C} = 12.25 Hz), 32.21 (s, C(CH₃)₃), 31.1 (s, br, COD, methylene), 30.28 (s, CMe₃).

Data for **2b** are as follows. Anal. Calcd for C₃₆H₆₀PtRh₂Si₄: C, 42.98; H, 5.96. Found: C, 42.53; H, 5.99. MS (FAB⁺): *m/z* 1006 (M⁺, 66%), 897 (M⁺ - COD, 35%). IR (cm⁻¹): ν(C≡C) 1965 (vs), 1948 (vs). ¹H NMR (CDCl₃, δ, 15 °C): 4.79 (s, br, 8H, COD, olefinic), 2.34 (m, br, 8H, COD, methylene), 1.96 (m, 8H, COD, methylene), 0.2 (s, 36H, SiMe₃); at -50 °C, 4.76 (hump, COD, olefinic), 2.34 (br, COD, methylene), 1.94 (br, COD, methylene), 0.17 (s, SiMe₃). ¹³C NMR (CDCl₃, δ, 15 °C): 123.93 (C_α, C_α≡C_βSiMe₃, ¹J_{Pt-C} = 752.2 Hz), 105.99 (C_β, C_α≡C_βSiMe₃, ²J_{Pt-C} = 235 Hz), 82.01 (d, COD, olefinic, J_{Rh-C} = 13.3 Hz), 30.92 (s, COD, methylene), 1.26 (s, SiMe₃); at -50 °C, C_α and C_β are not observed, 79.7 (br, COD, olefinic), 31.06 (s, br, COD, methylene), 1.36 (s, SiMe₃).

Preparation of {Pt(μ-C≡CBu^t)₄[Rh₂(μ-Cl)(COD)]₂} (3a**).** To a solution of **2a** (0.20 g, 0.21 mmol) in diethyl ether (20 mL) at -20 °C was added [Rh(μ-Cl)(COD)]₂ (0.10 g, 0.20 mmol), and the mixture was stirred at low temperature for 15 min. During this time the complex [Rh(μ-Cl)(COD)]₂ slowly dissolved, resulting in the formation of a deep orange solution. After another 15 min of stirring at room temperature an orange solid precipitated. The mixture was further stirred for 3 h, and the resulting orange solid was filtered off and washed with Et₂O. Yield: 0.22 g (72%).

Anal. Calcd for C₅₆H₈₄Cl₂PtRh₄: C, 46.88; H, 5.86. Found: C, 46.87; H, 5.05. MS (FAB⁺): molecular peak not observed, *m/z* 941 ([Pt(C≡CBu^t)₄Rh₂(COD)]⁺, 4.7%), 833 ([Pt(C≡CBu^t)₄-Rh₂(COD)]⁺, 90%). IR (cm⁻¹): ν(C≡C) 2022 (s). ¹H NMR (CDCl₃, δ, 30 °C): 4.61 (br, 16 H, COD, olefinic), 2.39 (s, br, 16 H, COD, methylene), 1.74 (d, 16 H, COD, methylene), 1.51 (s, 36 H, Bu^t); at 15 °C, 4.55 (vbr, 16 H, COD, olefinic), 2.37 (s, br, 16 H, COD, methylene), 1.72 (d, 16 H, COD, methylene), 1.49 (s, 36 H, Bu^t); at -50 °C, 5.44 (4H), 4.64 (4H), 4.06 (4H), 3.95 (4H) (br, COD, olefinic), 2.44, 2.19 (br, 16H), 1.76, 1.62 (br, 16 H) (COD, methylene), 1.45 (s, 36 H, Bu^t). ¹³C NMR (CDCl₃, δ, -50 °C): 102.14 (C_β, C_α≡C_βBu^t, ²J_{Pt-C} = 292.6 Hz), 84.1 (m, COD, olefinic), 80.98 (C_α, C_α≡C_βBu^t, ¹J_{Pt-C} = 934.5 Hz), 76.57 (br, COD, olefinic, this signal overlaps with the chloroform signal), 32.68 [s, C(CH₃)₃], 31.25 (s, CMe₃), 30.22 (hump, COD, methylene), 28.82 (hump, COD, methylene).

Preparation of {Pt(μ-C≡CBu^t)₄[Rh₂(μ-OH)(COD)]₂} (4a**).** A solution of **2b** (0.210 g, 0.21 mmol) in THF (20 mL) at -20 °C was treated with [Rh(μ-OH)(COD)]₂ (0.100 g, 0.22 mmol), and the mixture was stirred at low temperature for 15 min. Following this, the mixture was warmed to reach room temperature and was stirred for 3 h. The resulting deep orange solution was evaporated to dryness, and 10 mL of acetone was added, yielding an orange solid, which was filtered off and washed with acetone (~3 mL). Yield: 0.223 g (76%).

Anal. Calcd for C₅₆H₈₈O₂PtRh₄: C, 48.05; H, 6.29. Found: C, 47.88; H, 6.67. MS (FAB⁺): molecular peak not observed, *m/z* 1272 ([M - COD - OH]⁺, 16%), 941 ([Pt(C≡CBu^t)₄-Rh₂(COD)]⁺, 37%), 833 ([Pt(C≡CBu^t)₄Rh₂(COD)]⁺, 67%). IR (cm⁻¹): ν(OH) 3602 (m), ν(C≡C) 2021 (s). ¹H NMR (CDCl₃, δ, 15 °C): 4.53 (s, br, 8 H, COD, olefinic), 3.81 (s, br, 8 H, COD, olefinic), 2.34 (br, 16 H, COD, methylene), 1.67 (m, 16 H, COD, methylene), 1.52 (s, 36 H, Bu^t), -3.01 (s, 2H, OH); at -50 °C, 4.7 (vbr, 8 H, COD, olefinic), 3.77 (vbr, 8H, COD, olefinic), 2.30

(11) Ara, I.; Berenguer, J. R.; Fornies, J.; Lalinde E.; Martínez, F. *XV Meeting of the Spanish Organometallic Chemistry Group*, Sevilla, 1995.

(12) Ara, I.; Berenguer, J. R.; Eguizabal, E.; Lalinde, E.; Fornies, J. Unpublished results.

(13) Espinet, P.; Fornies, J.; Martínez, F.; Tomás, M.; Lalinde, E.; Moreno, M. T.; Ruiz, A.; Welch, A. J. *J. Chem. Soc., Dalton Trans.* **1990**, 791.

Table 3. Crystallographic Data and Structure Refinement Parameters for Complexes 3a and 4a^a

	3a	4a
empirical formula	C ₅₆ H ₈₄ Cl ₂ PtRh ₄	C ₅₆ H ₈₆ O ₂ PtRh ₄
fw	1434.86	1397.98
cryst syst	orthorhombic	monoclinic
space group	<i>Pbca</i>	<i>C₂/c</i>
unit cell dimens	<i>a</i> = 20.120(2) Å <i>b</i> = 23.468(3) Å <i>c</i> = 23.567(3) Å	<i>a</i> = 14.784(5) Å <i>b</i> = 17.091(6) Å <i>c</i> = 21.054(8) Å
	α = 90° β = 90° γ = 90°	α = 90° β = 95.86(3)° γ = 90°
<i>V</i> , Å ³	11128(2)	5292(3)
<i>Z</i>	8	4
density (calcd), Mg/m ³	1.713	1.755
abs coeff, mm ⁻¹	3.797	3.894
<i>F</i> (000)	5696	2784
cryst size, mm	0.40 × 0.28 × 0.14	0.50 × 0.50 × 0.50
temp, K	200(1)	298(1)
wavelength, Å	0.71073	0.71073
2θ range for data collection, deg	4–48	3–46
index ranges	–23 ≤ <i>h</i> ≤ 2 0 ≤ <i>k</i> ≤ 26 0 ≤ <i>l</i> ≤ 26	–16 ≤ <i>h</i> ≤ 16 0 ≤ <i>k</i> ≤ 18 0 ≤ <i>l</i> ≤ 23
no. of rflns collected	9299	3775
no. of indep rflns	8607	3656
no. of data/restraints/params	7169/6/571	3656/0/288
goodness of fit on <i>F</i> ²	1.054	1.023
weighting parameters <i>g</i> ₁ , <i>g</i> ₂	0.0347, 14.3247	0.0404, 16.1089
<i>R</i> indices (<i>I</i> > 2σ(<i>I</i>))	<i>R</i> 1 = 0.0532, <i>wR</i> 2 = 0.0877	<i>R</i> 1 = 0.0396, <i>wR</i> 2 = 0.0816
<i>R</i> indices (all data)	<i>R</i> 1 = 0.1347, <i>wR</i> 2 = 0.1267	<i>R</i> 1 = 0.0567, <i>wR</i> 2 = 0.0871
mean, max shift/esd , f. cycle	0.000, 0.000	0.000, 0.001
largest diff peak and hole, e/Å ³	1.564 and –1.095	0.851 and –0.706

^a *R*1 = Σ(|*F*_o – |*F*_c||)/Σ|*F*_o|. *wR*2 = [Σ*w*(|*F*_o – |*F*_c||)²]/[Σ*w*|*F*_o|²]^{1/2}. Goodness of fit = [Σ*w*(|*F*_o – |*F*_c||)²/(*N*_{obs} – *N*_{param})]^{1/2}. *w* = [σ²(*F*_o) + (*g*₁*P*)² + *g*₂*P*]⁻¹; *P* = [max(*F*_o²; 0) + 2*F*_c²]/3.

(br, 16H, COD, methylene), 1.64 (br, 16 H, COD, methylene), 1.48 (s, 36 H, Bu^t). ¹³C NMR (CDCl₃, δ, –50 °C): 106.68 (C_β, C_α≡C_βBu^t), 78.83 (C_α, C_α≡C_βBu^t, ¹*J*_{Pt–C} = 919.3 Hz), 74.23 (d, COD, olefinic, *J*_{Rh–C} = 11.7 Hz), 32.61 [s, C(CH₃)], 31.62 (s, CMe₃), 31.31 (s, COD, methylene).

X-ray Crystal Structure Determination of {Pt(μ-C≡CBu^t)₄[Rh₂(μ-Cl)(COD)₂]₂} (3a). Suitable crystals of **3a** were obtained by slow diffusion of a dichloromethane solution of **3a** over *n*-hexane at –30 °C. A representative cube-shaped orange crystal was fixed with epoxy on top of a glass fiber and mounted on a four-circle Siemens P4 autodiffractometer (graphite-monochromated Mo Kα radiation). Data were collected at 200 K by the ω-scan method (4 < 2θ < 48°). Three check reflections, measured every 350 reflections, showed no decay of intensity at the end of data collection. Data were corrected for Lorentz and polarization effects. In addition, an absorption correction based on ψ scans (8 reflections) was applied.

The structure was solved by the heavy-atom method, which revealed the positions of the platinum and rhodium atoms. The remaining non-hydrogen atoms were located in succeeding difference Fourier syntheses and subjected to anisotropic full-matrix least-squares refinement. H atoms were included at calculated positions and refined with isotropic thermal parameters being 1.2 times those of the corresponding C atoms, except all CH₃ hydrogens, which were refined with a common isotropic thermal parameter. Final residuals were *R* = 0.0532 and *R*_w = 0.1348. The highest peaks in the final difference map (four peaks between 1.56 and 1.12 e/Å³) are close to the heavy atoms and have no chemical significance.

X-ray Crystal Structure Determination of {Pt(μ-C≡CBu^t)₄[Rh₂(μ-OH)(COD)₂]₂} (4a). Suitable crystals of **4a** were obtained by slow evaporation of a chloroform solution of **4a** over isopropyl ether. A representative cube-shaped orange crystal was sealed inside a thin-walled glass capillary with epoxy and mounted on a four-circle Nicolet autodiffractometer (graphite-monochromated Mo Kα radiation). Data were collected at room temperature by the ω-scan method in two shells (3 < 2θ < 40° and 40 < 2θ < 46°). Six check reflections,

measured every 300 reflections, showed a decay of 10% at the end of data collection. Data were corrected for Lorentz and polarization effects, and an absorption correction based on ψ scans (7 reflections) was also applied.

The structure was solved by the heavy-atom method, which revealed the positions of the platinum and rhodium atoms. The remaining non-hydrogen atoms were located in succeeding difference Fourier syntheses and subjected to anisotropic full-matrix least-squares refinement. H atoms were added at calculated positions and refined with isotropic thermal parameters being 1.2 times those of the corresponding C atoms, except all CH₃ hydrogens, which were refined with a common isotropic thermal parameter. Final residuals were *R* = 0.0396 and *R*_w = 0.0871. There is no electron density above 1 e/Å³ in the final difference map.

Crystallographic parameters for both complexes are given in Table 3. All calculations were performed on a local area VAX cluster with the SHELXTL PLUS and SHELXL 93 software packages.^{14,15}

Acknowledgment. We thank the Comisión Interministerial de Ciencia y Tecnología (Spain, Project PB 95-003CO2 - O1, O2) for financial support. E.L. and J.R.B. also thank the Universidad de La Rioja for financial support.

Supporting Information Available: Tables of atomic coordinates, anisotropic displacement parameters, hydrogen atom positional parameters and *U* values, and complete bond lengths and angles for **3a** and **4a** (20 pages). Ordering information is given on any current masthead page.

OM9702587

(14) SHELXTL-PLUS, Software Package for the Determination of Crystal Structures, Release 4.0; Siemens Analytical X-ray Instruments, Inc., Madison, WI, 1990.

(15) Sheldrick, G. M. SHELXL-93: FORTRAN Program for The Refinement of Crystal Structures from Diffraction Data; University of Göttingen, Göttingen, Germany, 1993.